Safe Tumbling of Heavy Objects Using a Two-Cable Crane

by

Cormac O'Neill

B.S., California Institute of Technology (2019)

Submitted to the Department of Mechanical Engineering
in partial fulfillment of the requirements for the degree of

Master of Science in Mechanical Engineering

at the

MASSACHUSETTS INSTITUTE OF TECHNOLOGY

June 2021

Author .....
Department of Mechanical Engineering
May 14, 2021

Certified by .....
Haruhiko Harry Asada
Ford Professor of Engineering, Department of Mechanical Engineering
Thesis Supervisor

Accepted by .....
Nicolas G. Hadjiconstantinou
Professor of Mechanical Engineering, Graduate Officer

Safe Tumbling of Heavy Objects Using a Two-Cable Crane

by

Cormac O'Neill

Submitted to the Department of Mechanical Engineering
on May 14, 2021, in partial fulfillment of the
requirements for the degree of
Master of Science in Mechanical Engineering

Abstract

In heavy industries, large, heavy objects must be tumbled to access features on their bottoms and sides for assembly and maintenance. Traditional manual operations using a single-cable crane are high-risk, and difficult for less experienced workers. Automating the tumbling process is made challenging due to the presence of kinematic and static singularities which are shown to occur when a single-cable crane loses control over the block being tumbled. Here, an autonomous method for safely tumbling a heavy block sitting on a surface using a two-cable crane is presented. Two winches controlling a pair of cables on a crane are coordinated in such a way that a) the block cannot slip on the floor, b) the block is not lifted into the air, and c) the block is under quasi-static balanced control at all times. A control algorithm for coordinating the two winches is developed for safely tumbling a block without slipping or becoming airborne as well as for eliminating the effect of singularities. A small-scale prototype is developed and the control algorithm is implemented and evaluated experimentally.

Thesis Supervisor: Haruhiko Harry Asada
Title: Ford Professor of Engineering, Department of Mechanical Engineering

Acknowledgments

I would like to thank Prof. Harry Asada, my thesis supervisor for helping me and guiding me through the entire process of this research project and thesis preparation. I would like to thank all of my fellow researchers at the d'Arbeloff Laboratory for all their help and camaraderie during my time as a master's degree student, especially Rachel Hoffman-Bice and Eisuke Matsuzaki for their mentorship and support.

Contents

List of Figures

Chapter 1

Introduction

Heavy manufacturing industries are finding it increasingly difficult to recruit new workers. The nature of labor-intensive roles on the factory floor has led to these jobs being considered dangerous and difficult, discouraging new workers from entering the field [1]. The use of overhead cranes in close proximity to human workers is a particular source of risk [2]. Such roles require highly skilled workers, many of whom are leaving the industry. This problem is compounded by the aging populations of many industrialised countries. While increased automation is a potential solution to the growing labor shortage, contemporary industrial robots struggle to provide the fine manipulation and high payload capacities required by heavy industry manufacturing techniques.

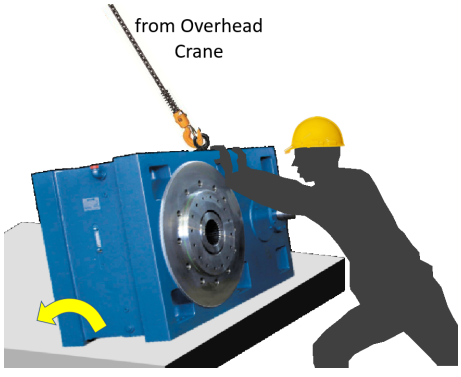

Figure 1-1: Workers must often work with cranes in order to tumble heavy objects about a contact point on the ground. This is done to gain access to otherwise obscured faces of the object.

Applying traditional industrial robots to heavy industries has been limited to high-volume productions of relatively small, lightweight products. Robots for handling over one hundred kilograms of payload are bulky, cost prohibitive, and inflexible, limiting their widespread adoption within the field. A promising alternative is the use of automated cranes which can not only transport heavy objects, but also manipulate in multiple degrees of freedom. In particular, cable-suspended parallel robots (CSPRs) have been studied extensively in prior work, and new designs for such manipulators continue to be developed [3]. Prominent examples include the quadcopter-deployed Flycrane [4] and the NIST Robocrane [5]. However, these CSPRs have limited dexterity. A particular challenge for underactuated CSPRs is their reliance on gravity to provide tension for their cables [6]. Fully actuated cable robots avoid this problem through additional cables, although the need to prevent interference between the cables and the environment provide an incentive to keep the number of cables low [3].

Recent work in the field of robotic manipulation has explored novel control strategies that take advantage of the surrounding environment through "extrinsic dexterity" [7, 8]. For example, an articulated robot can re-grasp an object by exploiting the surrounding environment surface as a type of jig or fixture [9]. The possibility of expanding the use of extrinsic dexterity to cable robots has started to be explored, such as by using external contact to expand the robot's workspace [10] or to solve a unique manipulation challenge like the precision insertion of heavy objects using a multi-cable crane [11]. Exploiting contact with environment will expand the manipulative capability of robots, and such strategies can also be applied to multi-cable cranes.

This paper addresses a new type of manipulation challenge where an object is manipulated with a multi-cable crane by exploiting environmental contacts. Specifically, tumbling of heavy objects on a flat surface, as illustrated in Fig. 1-1, is considered. Tumbling is a particularly dangerous task for workers, since the heavy object goes through an unstable equilibrium in the middle of the operation. Furthermore, the heavy object may slip on the surface, if it is pulled improperly, and if the object loses contact with the surface and goes into the air, it can swing dangerously. The object

behavior is governed by its frictional interface with the surface, and the force generated by the cable is subject to unidirectional loading constraints; cables go slack when compressed. At least 2 cables are necessary to overcome the unidirectional loading constraints, and the multiple cables must be coordinated to tumble an object safely.

With a 2-cable CSPR, we demonstrate that a cubic block can be safely rotated 90 degrees about an edge in contact with the ground, without the block slipping or being lifted into the air. In the following sections, we investigate the behavior of the block and analyze singularities that occur during tumbling operations. During tumbling, the block is subject to floor contact and gravity, and it is manipulated by cables with unidirectional loading constraints. An effective control algorithm is developed and tested on a prototype.

Chapter 2

Approach

2.1 Tumbling Process

Various heavy objects are processed and assembled in heavy industry factories. Among diverse shapes of objects, rectangular blocks as illustrated in Fig. 1-1 represent a typical shape, e.g. engine cylinder blocks and large gearbox cases. To tumble such a rectangular block a cable is attached to an edge of the top surface and the block is rotated about its bottom edge. In the current work, the geometry of the block is simplified to a square, and its motion is assumed to be constrained within a vertical plane.

Fig. 2-1 shows a schematic of the tumbling process. The goal is to rotate the square block of side length L and mass M about the origin O. The process starts at the rotation angle $\gamma = 0$ and ends at $\gamma = \frac{\pi}{2}$ $(90°)$. The center of mass is assumed to be in the middle of the block. The reaction force at the pivotal point O is decomposed to normal force N and friction f_d. The winch of a crane (not shown in the figure) pulls the block at point A on the block with force F in the direction θ measured from the horizontal axis. The location of the winch, point B, and the cable-attachment point A are described with the parameters shown in the figure.

For automated tumbling to be acceptable within industry settings, safety must be of paramount importance. To successfully perform a safe tumbling operation, we enforce three conditions:

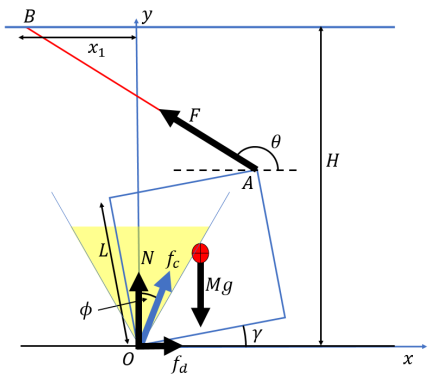

Figure 2-1: Force balance diagram for planar tumbling with key dimensions shown. L is the side length of the square block, F is the applied external force, θ is the angle of the applied external force, γ is the angle of the block, O is the origin of the system at the bottom left corner of the block, H is the height of the cable-platform attachment point, and x_1 is the x coordinate of the cable-platform attachment point. In addition, we define ϕ as the angle of the resultant force, f_c, on the lower left corner of the block due to friction, f_d, and the normal force, N. This angle must remain within the yellow friction cone shown in order for the block to not slip during tumbling.

- The block must not slip along the ground;
- The block must not be lifted into the air; and
- The tumbling process is quasi-static at all times.

No slipping is a fundamental requirement for accomplishing the tumbling operation as well as for safety of operation. The no-slip condition can be stated by using the friction cone in Fig. 2-1. Let ϕ be the angle between the normal force at the floor contact and the resultant reaction force including the friction. This angle must remain within the friction cone determined by the static friction coefficient μ.

$$|\phi| < \arctan(\mu) \tag{2.1}$$

If the block were lifted into the air, it would swing dangerously. The no-lift condition is met if the normal force N acting at the contacting edge is kept positive at all times:

$$N > 0 \tag{2.2}$$

Furthermore, the last condition, quasi-static operation, assures that no significant acceleration is generated in the tumbling operation.

$$\ddot{\gamma} \approx 0 \tag{2.3}$$

This implies that the inertial force is negligibly small, and that the static balance conditions are maintained throughout the process. Otherwise, the block may be accelerated and hit other objects or impact the floor, causing damage.

2.2 Singularity

During tumbling, the cable force is applied to generate a moment about the pivotal point O in order to balance the moment produced by gravity. However, if the force is applied through only a single cable to the tumbling block, there are two cases in which quasi-static balance control cannot be achieved.

The first case occurs at the unstable equilibrium where $\gamma = \frac{\pi}{4}$ (45°), as shown in Fig. 2-2a. At this configuration, the block's weight does not produce a moment that counter-acts the moment from the cable. Therefore, the single cable cannot control the quasi-static process. With a cable set from the left (shown in the broken arrow in Fig. 2-2a), the cable cannot generate a clockwise moment due to the unidirectional loading constraint. If the cable pulls the block from the same direction, it creates a counter-clockwise moment, but the block falls and the cable cannot stop it. The block is not controllable at this configuration with a single cable. This particular configuration is referred to as the gravity singularity.

The second singularity occurs when the cable's line of action passes through the pivotal point, preventing the cable tension from generating a moment about it, as shown in Fig. 2-2b. As the block is rotated, the distance between the pivot and the line of cable force varies; the moment reduces to zero as it approaches this particular point where the cable line and the pivot point align. If the center of mass is still generating a finite moment when this occurs, moment balance fails and the robot is unable to maintain quasi-static balance control over the block. We call this occurrence

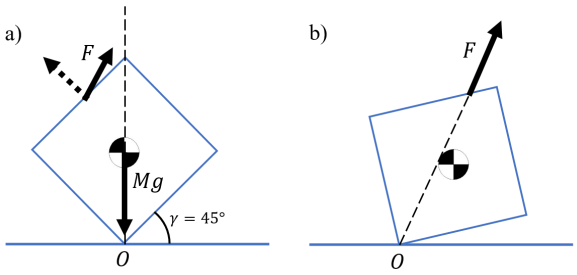

Figure 2-2: (a) Depiction of a gravity singularity when the block's center of mass is directly above the pivot point. (b) Depiction of a cable singularity when the applied force is colinear with the pivot point.

the cable singularity.

Because of these two types of singularity, tumbling with a single winch is unsatisfactory with respect to the three safety conditions described previously. The winch inevitably loses control over the tumbling process as it hits these singularity configurations. No matter where the winch is placed, the tumbling process either gets stuck near a singular configuration, or violates the quasi-static condition, leading to dangerous movements.

We propose a dual-cable crane robot to resolve the singularity problems associated with the tumbling of a block contacting a floor.

Chapter 3

Coordinated Dual-Cable Winch Control

3.1 No-Slip, No-Lift Conditions

Fig. 3-1 shows the tumbling process using two cables. Each cable winch applies a tension T_i from angle $\theta_i, i = 1, 2$. The resultant force generated by the two cables is given by

$$F_x = T_1 \cos\theta_1 + T_2 \cos\theta_2 \tag{3.1}$$

$$F_y = T_1 \sin\theta_1 + T_2 \sin\theta_2 \tag{3.2}$$

$$F = \sqrt{F_x^2 + F_y^2} \tag{3.3}$$

where

$$T_1 \geq 0, T_2 \geq 0 \tag{3.4}$$

The two cables can generate an arbitrary force $F \geq 0$ in a direction between the two cables: $\theta \in [\theta_2, \theta_1]$. The resultant force and its direction must be determined so that the safety requirements, no-slip and no-lift conditions, may be satisfied.

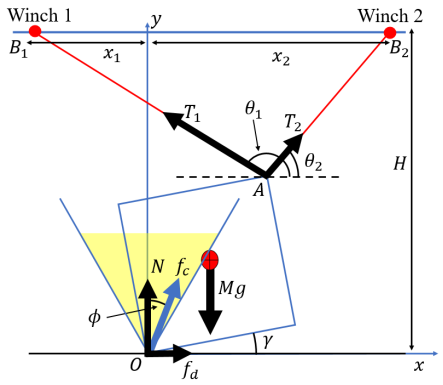

Figure 3-1: Force balance diagram for planar tumbling with 2 cables.

From the static force and moment balance conditions, the normal force N and the direction of the floor reaction force, ϕ, are given by

$$N = Mg - F\sin\theta > 0 \tag{3.5}$$

$$\phi = \arctan\left(-\frac{F\cos\theta}{N}\right) \tag{3.6}$$

In order to maintain the no-lift and no-slip conditions, it is desirable that angle ϕ is close to 0 and normal force N is close to Mg. The question is how to determine the resultant cable force and its direction, F and θ, so that ϕ is small and N is close to Mg.

To find an optimal cable force, we consider the following penalty function:

$$J = \left(\frac{\phi}{\arctan(\mu)}\right)^2 + \left(\frac{Mg - N}{Mg}\right)^2 \tag{3.7}$$

The penalty becomes zero when the reaction force from the floor has no friction, that is, $\phi = 0$, and the normal force is the same as the gravity force of the block. We determine an optimal resultant cable force, i.e. the magnitude F and direction θ, that minimizes the penalty.

$$(F^o(\gamma), \theta^o(\gamma)) = \underset{\substack{F\geq 0 \\ \theta\in(\theta_2,\theta_1)}}{\arg\min}\, J(F, \theta; \gamma) \tag{3.8}$$

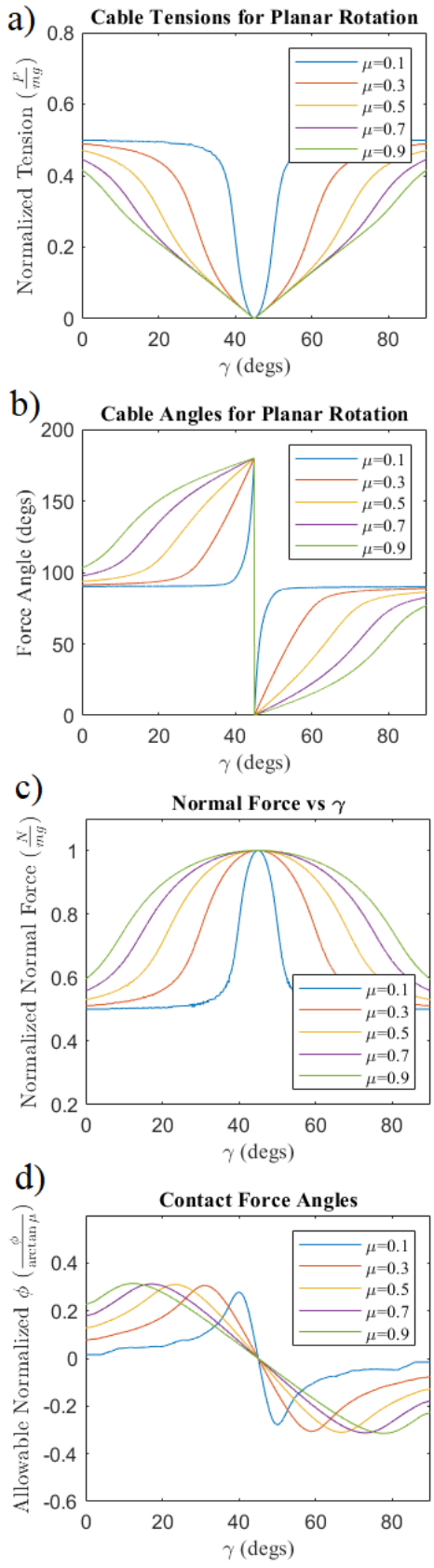

Figure 3-2: Results of simulated quasi-static tumbling with a resultant cable force over a range of values for μ.

Note that, by varying the two cable tensions, T_1, T_2 , the resultant force can be directed in an arbitrary direction between θ_1 and θ_2, the directions of cables 1 and 2, respectively.

The optimal cable force and its direction vary depending on the tumbling angle γ. Fig. 3-2 shows the optimal resultant cable force against γ for a range of μ values. We observe that a trade-off occurs between the selected pairs of F and θ, with a preference for larger forces being applied at angles close to 90° at the start and end of tumbling. This is due to the greater moment being applied by the block's center of mass when it is further from the pivot point, requiring a larger F in order to be balanced. In order to avoid slipping, the larger F is preferentially directed vertically, resulting in F being directed in angles close to $\theta = 90^\circ$. However, as the block approaches $\gamma = 45^\circ$, a smaller force is capable of providing the required torque. The smaller force can be applied at an angle closer to the horizontal without risking the no slip condition. In turn, this increases the normal force at the pivot point, reducing the risk of the no lift condition being violated. This general trade off results in the no slip condition being dominant closer to $\gamma = 0^\circ e$ and $\gamma = 90^\circ$, while the no lift condition is dominant about $\gamma = 45^\circ$.

By performing the optimization for a range of friction coefficients μ, we are able to evaluate how the tumbling operation is susceptible to changes in its environment (Fig. 3-2). Lower frictional coefficients make it harder to prevent slipping during tumbling, which causes the transition to a dominant no lift condition to occur later and more sharply. In fact, as $\mu \to 0$ there is little room for a trade-off to occur between the values of N and ϕ, as F and θ's selection is almost entirely determined by the no slip condition.

Another key observation from the simulation is the response of the system to the singularity at $\gamma = 45^\circ$ where the block's gravity force is not generating any torque about the pivot. This means that the x-component of the applied force must be equal to zero, which is achievable by having $\theta = 90^\circ$, $F = 0$, or both. As shown in Fig. 3-2b, across the singularity, the cable angle θ changes discontinuously between 0° and 180° as the direction of the balancing moment generated by the cable must flip

instantaneously.

3.2 Static Controllability and Hand-Over Protocol

At the singular point, the gravity moment vanishes, and the robot loses static controllability, i.e. the ability to quasi-statically control the tumbling angle γ through static balancing. At the singular point, static balance can be achieved with zero cable tensions; both cables go slack. But, the unidirectional nature of load bearing property does not allow the cables to control the tumbling angle. This problem can be solved by applying a bias tension T_0 to the cables. Suppose that at the singular point the cable angles are the same, $\theta_1 = \theta_2$. Applying the same bias force to both cables, the resultant force of the two cables has no x-component; it points in the vertical direction. Small changes from this static balance allow the robot to move the block quasi-statically left and right. Thus, the robot can maintain the static controllability in the vicinity of the singular point.

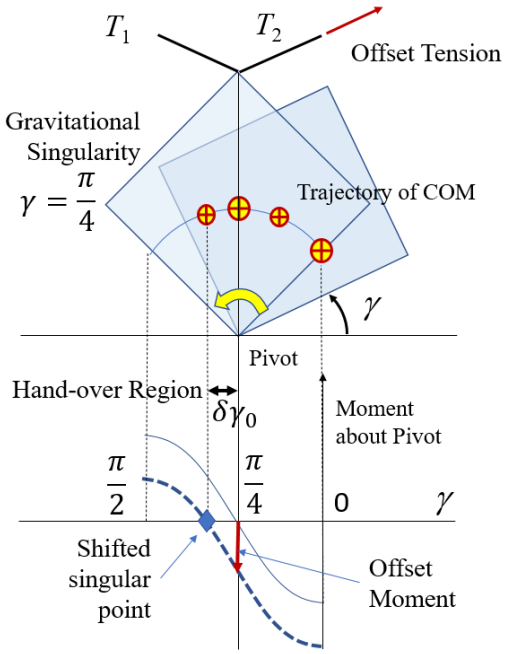

Figure 3-3: The application of an off-set (bias) force in the follower cable shifts the point of zero moment about the pivot away from $\gamma = 45°$.

A characteristic behavior of the tumbling process is that all variables are sym-

metric with respect to the singular point, as manifested in Fig. 3-2. The role of the two cables swap at the singular point. Cable 1 bears most of the load for the first half, and Cable 2 takes it for the second half. In the middle, Cable 1 transitions the load to Cable 2. We refer to the cable bearing the majority of the load as the leader, while the other cable is the follower. Suppose that Cable 2 exerts a constant bias tension T_0 in the vicinity of the singular point. As shown in Fig. 3-3, the bias tension changes the moment about the pivot. Although the gravity moment alone vanishes at the singular point, the resultant force of the gravity and the bias tension produces a non-zero moment at $\gamma = 45°$. As a result, the zero moment point shifts to left, as shown by a blue diamond in the figure. Until this shifted point, the process is statically controllable. As γ gets closer to the shifted zero-moment point, the gravity force creates a significant counter-clockwise moment about the pivot. Then, Cable 2 can bear a significant load, taking the leader role from Cable 1. If no bias tension is applied, and the leader role is abruptly handed over to Cable 2 at $\gamma = 45°$, Cable 2 is unable to control the static balance. With the bias tension, the handover can take place after passing the original singular point, and a significant gravity moment builds up before Cable 2 takes over the leader role. Thus, the two winches can change the role in this Hand-Over region without losing the static controllability over the tumbling process.

3.3 Leader-Follower Control

The above Hand-Over Protocol leads us to adopt a leader-follower scheme for controlling the two cables in a simple, practical manner as well as to ensure the enforcement of the no-slip, no-lift, and static controllability conditions defined in section II. In this approach, depending on the phase of the tumbling operation, one of the cables is the leader and uses position control to rotate the block (Fig. 3-4). At the same time, the other cable (the follower) uses force control to maintain a positive tension to implement the Hand-Over Protocol and help ensure the static controllability throughout the process. A handover between the two cables is executed within the handover

region where the static controllability is guaranteed with use of a proper bias tension.

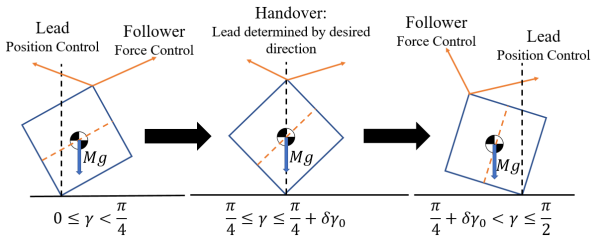

Figure 3-4: Diagram showing the outline of the leader-follower control approach, with the handover occurring at the gravity singularity at $\gamma = 45°$. $\delta\gamma_0$ references the hand-over region range shown in fig. 3-3.

We note that the use of two cables for planar tumbling comes with the added advantage of mitigating the vulnerability of a single-cable system to external disturbances. Due to the unidirectional loading capacity of cable members, disturbances that result in a compression force being applied to a single cable cannot be controlled using the tension controller feedback. However, a preloaded second cable oriented such that it is placed into tension when the initial cable would be compressed provides a way to resist such disturbances and maintain feedback control. This advantage is exploited in the leader-follower methodology by pretensioning the follower cable such that it maintains a constant tension.

Furthermore, combining position control and force control for the leader and follower winches provides a practical advantage for system integrity over pure force control for both winches. The position-controlled leader winch controls the progress of tumbling process by geometrically determining the configuration of the block, while the follower winch with force control assures the tension. The resultant force acting on the block may be different from its optimal magnitude and direction. Nevertheless, as long as the winches are placed properly so that the theoretical optimal conditions are best met, the resultant force acts within the region of no-slip and no-lifting conditions, as confirmed in the experiments in section 4.

The leader-follower control scheme presents a number of hyperparameters that need to be tuned. The positioning of the two winches, which defines the angle that the cables form with the horizontal during tumbling, and the bias tension applied to

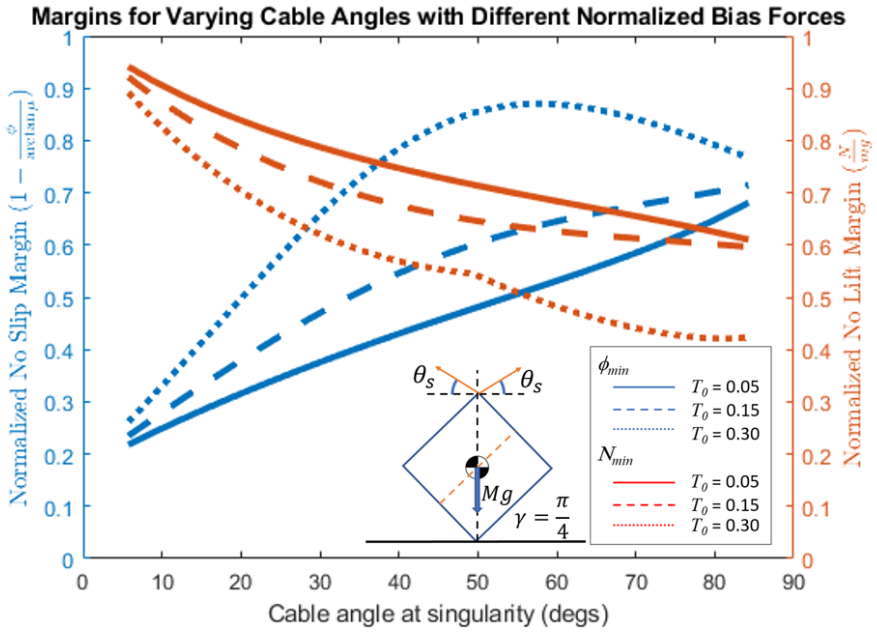

Figure 3-5: Simulated results from the leader-follower approach. Winch positioning (represented by cable angle) and the bias force in the follower cable (represented by tension force normalized by block weight in the legend) are shown to cause significant variations in the margins. The cable angle at singullarity plotted on the x-axis references the angle formed by the two cables at $\gamma = \frac{\pi}{4}$, as shown by θ_s in the diagram insert.

the follower cable are especially important for providing a safety margin that ensures that satisfaction of the no lift and no slip requirements. In fig. 3-5, the lowest no lift and no slip margins during a simulated tumbling operation are plotted over a range of winch locations (represented by the cable angles at the singularity, $\gamma = 45°$) and bias tensions.

The selection of cable angles presents a clear trade-off between the no slip and no lift requirements, with angles that are closer to the horizontal (0°) generally leading to lower no slip margins, but greater no lift margins. This implies that a particular set of cable angles would present an optimal balance between the two conditions. However, physical constraints on the CSPR setup may prevent certain angles from being feasible. This challenge can be overcome by varying the bias tension within the follower cable, since lower tension forces lead to a cross-over between the two margin curves with cable angles that are closer to vertical.

However, the behavior of the margin curves changes after the bias tension is increased beyond a certain point. Particularly high bias tensions (such as a normalized bias tension of 0.35, as in fig. 3-5) lead to the no slip margin peaking at certain cable angles. This occurs when the contact force passes through the vertical direction within the friction cone. While this leads to worse performance in the no lift sense, the potential for a significantly greater no slip margin may make such a selection worthwhile. Larger bias tensions also lead to greater offset moments and Hand-Over regions (fig. 3-3), which could be a worthwhile benefit despite reduced margins if there is significant uncertainty in the value of γ.

3.4 Pseudocode

Below, we present a pseudocode representation of the leader-follower control scheme which was implemented in hardware. The desired cable lengths for a given γ value were found using the inverse kinematics of the winchbot setup, which are reproduced here. Prior to implementing the control scheme, the bias tension $T_0 > 0$ must be selected. This bias tension must be chosen such that the no slip and no lift constraints

are maintained throughout the process. In the pseudocode, l_1 and l_2 are the cable lengths of winches 1 and 2, respectively. In addition, x_1, y_1, x_2, and y_2 are the x and y locations of winch 1 and 2. Finally, $\alpha = 45°$ is the angle between the base of the block, and a line drawn between the pivot and cable attachment points. $\delta\gamma$ is used to represent an uncertainty in the value of γ that is small enough such that when $\gamma = 45°$, $\gamma + \delta\gamma$ still lies within the Hand-Over region illustrated in fig. 3-3. The algorithm is as follows:

Pretension the cables using force control to remove slack.

$T_1 \leftarrow T_0$

$T_2 \leftarrow T_0$

Initialize with the initial cable lengths $l_{1,0}$ and $l_{2,0}$.

$l_1 \leftarrow l_{1,0}$

$l_2 \leftarrow l_{2,0}$

for $\gamma = (0, \pi]$ **do**

  if $\gamma < \frac{\pi}{2} + \delta\gamma$ **then**

    Winch 1 is the leader and winch 2 is the follower

    $T_2 \leftarrow T_0$

    $l_1 \leftarrow ((x_2 + \sqrt{2}L\cos(\pi - \gamma - \alpha))^2 + (y_2 - \sqrt{2}L\sin(\pi - \gamma - \alpha))^2)^{\frac{1}{2}}$

  else if $\gamma > \frac{\pi}{2} + \delta\gamma$ **then**

    Winch 2 is the leader and winch 1 is the follower

    $T_1 \leftarrow T_0$

    $l_2 \leftarrow ((x_1 + \sqrt{2}L\cos(\pi - \gamma - \alpha))^2 + (y_1 - \sqrt{2}L\sin(\pi - \gamma - \alpha))^2)^{\frac{1}{2}}$

  end if

  When $\gamma = \pi$ is reached, tumbling has been completed.

end for

Chapter 4

Implementation and Experiments

4.1 Controller Validation

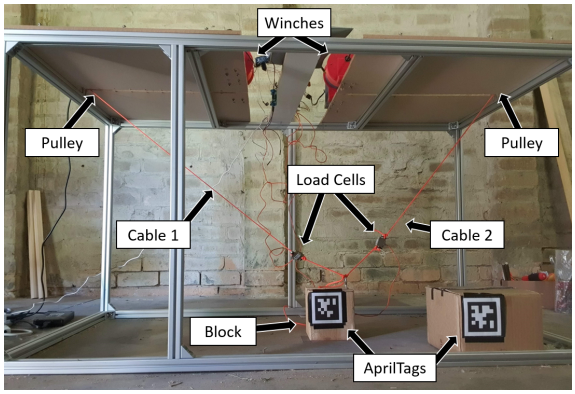

Figure 4-1: Photograph of the hardware setup used to implement the leader-follower methodology. AprilTags [12] have been implemented for validating the tumbling angle γ in post-processing, but they have not been used in the controller.

The proposed leader-follower control method was implemented on a small-scale prototype shown in Fig. 4-1, and the method was validated experimentally. The system consists of two winches controlling two independent cables connected to a single hook on a cubic block, which was tumbled along the ground. The setup allowed for the locations of the winches x_1 and x_2 to be varied discretely between operations. The length of the cables was monitored using motor encoders, while load cells monitored the tension within each cable. The control method was implemented in Simulink,

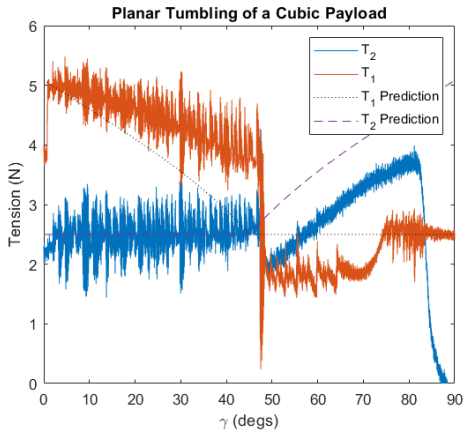

Figure 4-2: Recorded tensions compared to predictions during a tumbling attempt with the leader-follower methodology.

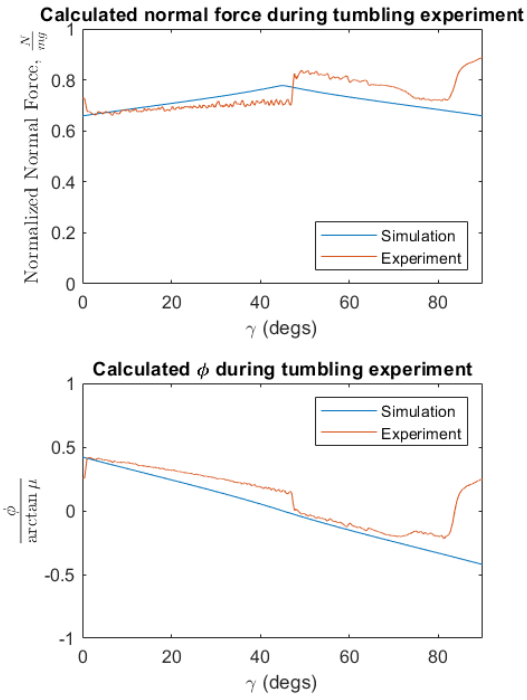

Figure 4-3: Leader-Follower tumbling results reparametrized to be in terms of F and θ, with the normalized cost function terms $\frac{\phi}{\arctan \mu}$ and $\frac{N}{mg}$. Predicted results from an idealized simulation are shown for comparison.

which was run in real time with a Raspberry Pi and Roboclaw motor controller. The hook was positioned in the cubic block such that its location along the block's top surface was $L = 0.145$m, and its perpendicular displacement from the top surface was 0.042m, although this displacement was not considered in the moment balance equations. The mass of the block was $M = 1.53$kg and the static friction coefficient was measured to be $\mu = 0.63$. Both cables were pretensioned prior to the tumbling process to prevent either cable from beginning the process with slack and potentially violating the quasi-static assumption made in this approach during the initial moments of operation.

Implementing the leader-follower control scheme described above, the block was tumbled from $\gamma = 0°$ to $\gamma = 90°$. The tensions in both cables were measured throughout the process and compared to those predicted in simulations as a means to verify the proposed control method; the raw result can be seen in Fig. 4-2. The general trend of the predicted tension profile is followed by both cables, and the application of the bias tension allows for the handover to occur successfully at the gravity singularity point midway through the process. However, the tension in cable 2 fails to reach the desired setpoint after the transition and results in the tensions in both cables being shifted lower.

This manifests itself in a noticeable drop in tension in the handover region around 45°. The model used to calculate the simulated tension profiles in Fig. 4-2 indicates that the tensions of both cables should equal each other when they switch roles, but instead we observe a gap in tensions between T_1 and T_2 before T_1 drops as it switches from leader to follower. Error in the estimated γ is the likeliest explanation for this observation, and changes to the timing of the handover process has been observed to affect the relative difference in tensions between the two cables. This measurement error would also explain the drop in tension after 80°, since we would see the block complete a tumble slightly earlier than expected. It was also observed that the winch actuating T_1 had difficulty maintaining higher tensions, leading to the offset in both T_1 and T_2 after 45°. However, the leader-follower system is able to mitigate both of these unexpected behaviours due to the offset tension in the follower cable providing

a buffer against unexpected variations in cable tensions.

To get a sense of how successful the leader-follower implementation is in ensuring the no slip and no lift conditions are met, we reparametrized the data in terms of the resultant force vector F and its angle θ. The reparametrization then enabled us to extract the values of ϕ and the normal force during the tumbling process (Fig. 4-3). In the normalized plots, we again see the impacts of the γ estimate error around 80° and 45°, but otherwise see that both the normalized normal force and ϕ follow a similar to trend to that predicted by the model. In fact, we can confirm that neither the no slip nor the no lift constraints are violated at any point during the tumbling process.

4.2 Failure Comparison

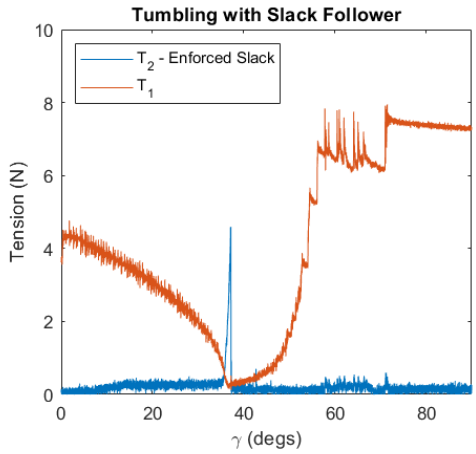

Figure 4-4: Tension results during tumbling attempt without a bias tension being set in cable 2. This results in a failure at the singularity, noticeable as a sudden peak in T_2 as control is lost and the block topples over.

To serve as a comparison to the successful implementation of the leader-follower controller, we experimentally investigated the failure mode that could otherwise have occurred during an attempted tumbling process: failure to maintain control at the singularity at $\gamma = 45°$. See Fig. 4-4.

A lack of control at the singularity is induced by enforcing a tension of 0N in the

follower cable, mimicking the performance of a single-cable, fixed winch design. This meant that the system was unable to balance the moments about the pivot point as the moment induced by the block's weight went to zero. Without the offset force from the follower cable creating a safe handover region, the block topples at $\gamma = 40°$. Toppling occurred prior to the singularity at 45° since the moment from the block's weight needed to only be less than that induced by the tension in the leader cable for failure to occur, rather than specifically zero. As shown in Fig. 4-4, this toppling can be seen in the tension profile as a sudden spike in T_2 as it suddenly bears the weight of the block before once again returning to the setpoint of 0N.

4.3 Varying the Follower Tension

To investigate the differences between the experimental results and expectations from the simulated model in section Controller Validation, further experiments were performed with an inertial measurement unit (IMU) attached to the block. The IMU was used to measure the value of γ during tumbling and comparing it to the estimated value of γ internally recorded by the feedforward leader-follower controller. The experimental setup used was otherwise a reconstruction of that shown in 4-1, but with different winch motors and load cells. A new setup was needed due to the researcher performing this experiment relocating internationally due to the impact of covid-19.

This setup was used to perform a number of tumbling operations with a range of different values for the follower cable's tension. By repeating the experiment for a range of follower tensions, we hoped to determine whether greater follower tensions would allow for the system to better recover from imperfect handovers due to errors in the estimated and actual value of γ. An example of one of these experiments is shown in fig. 4-5 with a follower tension of 9N. While we can see that tumbling was successful from the IMU measurements, the actual value of γ diverges from the estimate almost immediately and tumbling stops a few degrees earlier than desired. Of particular interest is a sudden shift in the gradient of the IMU measurements during the handover process. This is the result of the handover not occurring exactly

at the singularity due to the $/gamma$ error. However, the offset moment generated by the follower cable's tension is sufficient to prevent the failure of the tumbling operation and allows for control to be maintained, as intended. Note the significant difference between the measured value of γ at the handover, $\gamma = 42.75°$, and that of the singularity at $\gamma = 45°$.

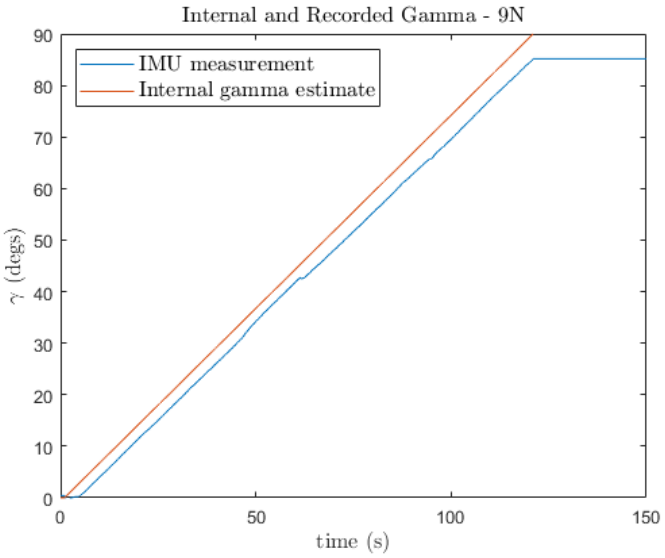

Figure 4-5: Values of the feedforward γ estimate used by the controller as well as that measured by an IMU. Tumbling was performed with a follower cable tension of 9N. Note that handover occurs prematurely as a result of errors between the estimated and actual γ values, but the controller is able to nevertheless complete the tumbling operation.

A close up of the shift in the measured γ gradient at the handover is presented in fig. 4-6. To quantify the ability of the system to recover from the premature handover, the drop in the measured γ angle and the time taken for the gradient of the IMU measurement to approximately return to its prior value were recorded. These properties are qualitatively identified within fig. 4-6. In addition to these values, we noted drop in follower tension at the handover which was recorded by the load cells, as shown in 4-7.

First we consider the drop in tension experienced for each of the tested follower tensions. Representing this drop as both an absolute drop in tension and a percentage of the follower cable's tension in fig. 4-8, we can see that the absolute drop in tension

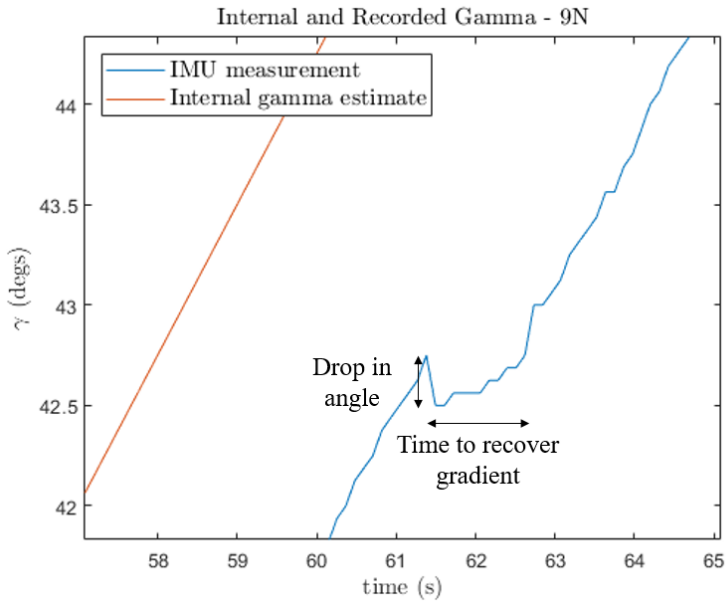

Figure 4-6: A closeup section of fig. 4-5. Two metrics used to quantify the severity of and recovery from the premature handover event are shown by way of labelling. The drop in angle is a sharp decrease in the value of γ immediately after the premature handover, and the time to recover gradient is the approximate time taken for the rate of tumbling to recover following the premature handover.

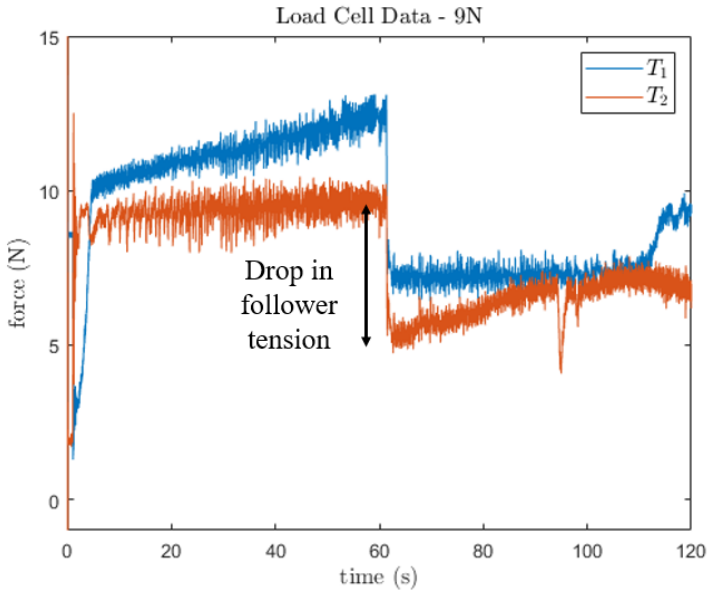

Figure 4-7: The tension values in both cables are shown with a follower tension of 9N. The drop in tension of the follower cable at the handover is indicated by a label. Note at higher follower tensions, it is expected for the lead cable's tension to increase as the handover is approached.

increases as the follower tension increases. However, the opposite trend is apparent when considering the tension drop as a percentage of the follower tension. This implies that larger follower tensions are better able to handle unexpected changes in cable loads without falling slack, a necessary behaviour in order to effectively overcome a premature handover. We also considered the drop in the angle at the handover in fig. 4-9. There was no clear trend linking the follower cable's tension and the change in angle at the premature handover. This is likely due to the position controlled cable dominating the angle drop as it attempts to vary the cable length for an inaccurate value of γ. However, in order to determine whether this increased buffer of cable tension leads to measurable improvements in premature handover handling, we investigate the time taken for the gradient of the IMU measurement to recover for the different follower tensions. We look to quantify this metric in two ways: an absolute length of time as depicted in fig. 4-10, and as the length of time taken per newton of follower tension, as in fig. 4-11. In both cases, we see a clear trend of the time taken to recover the rate of tumbling being reduced as the follower tension is increased. This supports our hypothesis that greater follower tensions allow for the system to better recover from the premature handover event resulting from inaccurate γ estimates.

Although the results of these experiments indicate that greater follower tensions enhance the system's ability to recover from premature handover events, we must recall that the follower tension cannot be increased without limit. Eventually, we would experience lifting, thereby violating one of the constraints established in section 2.1. The impact of increasing the follower tension on the no lift margin was explored in fig. 3-5, and these experiments reinforce the significance of the trade-off that must be performed between the no lift and no slip margins by way of selecting the follower cable's tension.

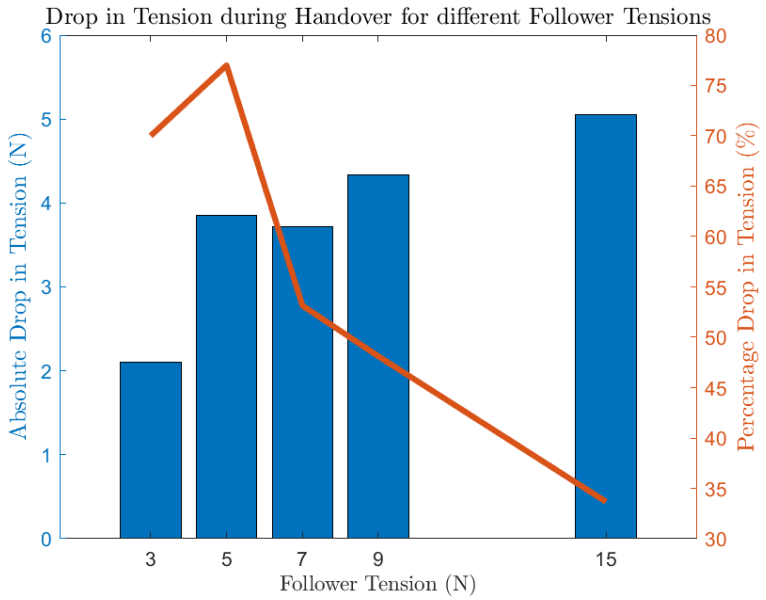

Figure 4-8: The drop in tension at the premature handover is shown as both an absolute drop in tension, and as a percentage of the follower tension setpoint, for a range of different follower tensions.

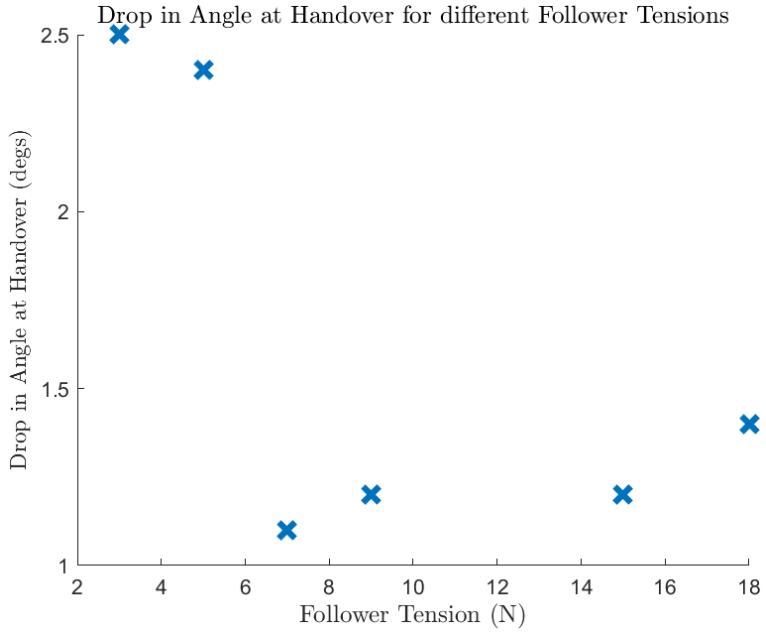

Figure 4-9: The change in γ angle at the premature handover is shown for a range of different follower tensions. No clear trend is identified between the two variables.

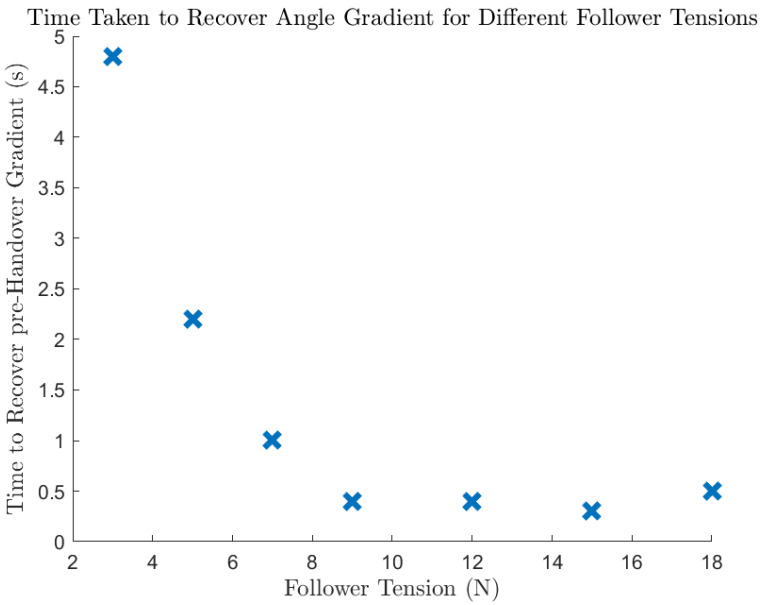

Figure 4-10: The time taken for the rate of tumbling (the gradient of the IMU measurements) to recover following a premature handover event is shown. It generally decreases as the follower tension is increased, although this effect is reduced at higher follower tensions.

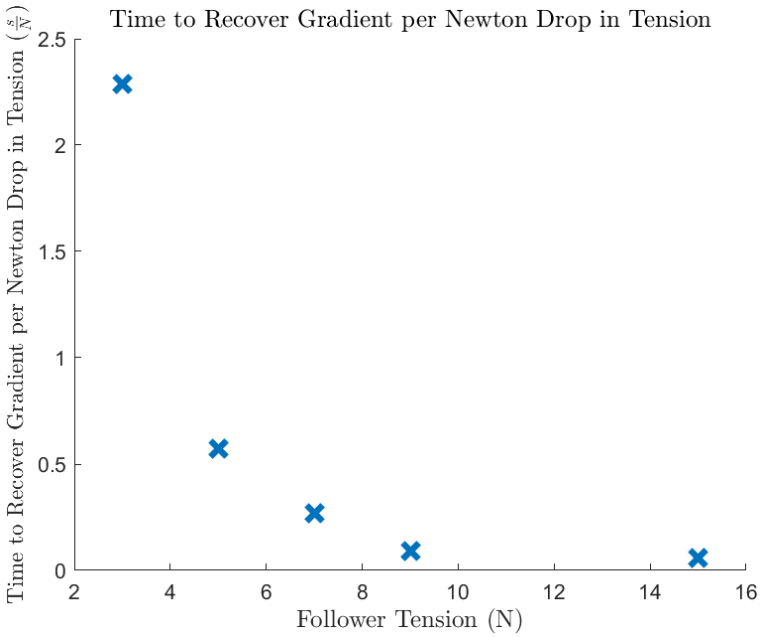

Figure 4-11: The time taken for the rate of tumbling (the gradient of the IMU measurements) to recover following a premature handover event, divided by the follower tension setpoint, is shown. It decreases as the follower tension is increased, although this effect is reduced at higher follower tensions.

Chapter 5

Conclusion

This paper presents a control method that allows an underactuated CSPR to tumble a cubic block. The unidirectional loading limitation of cables is overcome by using static friction from ground contact and a pair of cables to maintain positive cable tensions throughout the process. This two-cable approach allows for the system to be controllable even at the gravity singularity, $\gamma = 45°$, which would be impossible for a fixed-winch, single-cable setup. In our theoretical analysis of the system, we investigated how the tumbling operation could be optimized by controlling the values of F and θ for the resultant tension vector. A non-optimal, but safety-focused leader-follower implementation was demonstrated on hardware.

By varying the tension in a follower cable, a feedforward control system is shown to be able to recover from premature handovers caused by inaccurate tumbling angle (γ) estimates. However, it is shown through simulations that this follower cable tension must be carefully chosen so that it is not so high as to cause the block being tumbled to be lifted off of the ground.

We have identified a number of interesting avenues for future research into CSPR tumbling operations. Of particular interest is developing the current framework so that it can operate with more general payloads. Although the approach described here was tested for cubic payloads, the only geometric payload parameters that were used explicitly were the center of mass location, and the cable attachment location. These two parameters could be easily found for non-cubic payloads and allow for the

leader-follower control methodology to be expanded to the tumbling of more general payloads.

A limitation of the current work is the assumption that the tumbling operation is constrained to a two-dimensional plane. In order to ensure that there are no out-of-plane forces being applied to the block, the locations of the winches and the contact point on the block must all lie within a single vertical plane. Otherwise, an unwanted moment may rotate the block, violating the planar motion assumption. Work is being done to expand the 2-cable tumbling approach to a 3-cable CSPR. Such a design would help to alleviate the risk of out-of-plane forces, since the addition of an extra cable would allow for any such out-of-plane loads to be safely born without inducing any unwanted twisting of the block during tumbling.

The existing leader-follower tumbling framework could also be improved by introducing feedback to improve the estimation of γ during tumbling, and integrate this into the controller itself. This is apparent from the observation that premature handover events occur when a pure feedforward controller is implemented. An additional area of possible research would be the application of tumbling to aerial CSPRs. With the increasing prevalence of drones, such designs have become more popular within the literature [4]. Aerial CSPRs generally use fixed cable lengths and mobile drones rather than winches, presenting additional complexities when it comes to ensuring stable control during tumbling. But providing aerial CSPRs with the capability to perform more advanced manipulation tasks without additional hardware would enhance their utility in difficult-to-reach environments even beyond the factory floor.

External contact has also been explored as a means to aid with system identification by Fazeli et al. [13]. Implementing such a capability to autonomous cable robots that are already exploiting ground contact for manipulation could allow for improvements in both safety and performance. For example, an object could be successfully tumbled using the leader-follower approach despite key parameters such as the mass, being initially uncertain.

Bibliography

[1] Elka Torpey. *Got skills? Think manufacturing : Career Outlook: U.S. Bureau of Labor Statistics*. 2014. URL: https://www.bls.gov/careeroutlook/2014/article/manufacturing.htm (visited on 09/14/2019).

[2] Rodney G. Roberts, Todd Graham, and Thomas Lippitt. "On the inverse kinematics, statics, and fault tolerance of cable-suspended robots". In: *Journal of Robotic Systems* 15.10 (1998), pp. 581–597. DOI: 10.1002/(SICI)1097-4563(199810)15:10<581::AID-ROB4>3.0.CO;2-P. eprint: https://onlinelibrary.wiley.com/doi/pdf/10.1002/%28SICI%291097-4563%28199810%2915%3A10%3C581%3A%3AAID-ROB4%3E3.0.CO%3B2-P.

[3] Fereshteh Shahmiri and Russell Gentry. "A Survey of Cable-Suspended Parallel Robots and their Applications in Architecture and Construction". In: Dec. 2016, pp. 914–920. DOI: 10.5151/despro-sigradi2016-484.

[4] Dario Sanalitro et al. "Full-pose Manipulation Control of a Cable-suspended load with Multiple UAVs under Uncertainties". In: *IEEE Robotics and Automation Letters* PP (Jan. 2020), pp. 1–1. DOI: 10.1109/LRA.2020.2969930.

[5] Roger Bostelman et al. "Applications of the NIST Robocrane". In: *Proceedings of the 5th International Symposium on Robotics and Manufacturing*. Vol. 5. 1994, pp. 403–410.

[6] Xiaoqiang Tang. "An Overview of the Development for Cable-Driven Parallel Manipulator". In: *Advances in Mechanical Engineering* 6 (2014), p. 823028. DOI: 10.1155/2014/823028. eprint: https://doi.org/10.1155/2014/823028. URL: https://doi.org/10.1155/2014/823028.

[7] N. C. Dafle et al. "Extrinsic dexterity: In-hand manipulation with external forces". In: *2014 IEEE International Conference on Robotics and Automation (ICRA)*. 2014, pp. 1578–1585. DOI: 10.1109/ICRA.2014.6907062.

[8] Nikhil Chavan Dafle and Alberto Rodriguez. "Regrasping by Fixtureless Fixturing". In: *CoRR* abs/1809.08522 (2018). arXiv: 1809.08522. URL: http://arxiv.org/abs/1809.08522.

[9] N. Chavan-Dafle and A. Rodriguez. "Prehensile pushing: In-hand manipulation with push-primitives". In: *2015 IEEE/RSJ International Conference on Intelligent Robots and Systems (IROS)*. 2015, pp. 6215–6222.

[10] Antoine Martin, Stéphane Caro, and Philippe Cardou. "Design of a Cable-Driven Parallel Robot with Grasping Device". In: *Procedia CIRP* 70 (2018). 28th CIRP Design Conference 2018, 23-25 May 2018, Nantes, France, pp. 290–295. ISSN: 2212-8271. DOI: https://doi.org/10.1016/j.procir.2018.03.105. URL: http://www.sciencedirect.com/science/article/pii/S2212827118302609.

[11] R. Hoffman and H. H. Asada. "Precision Assembly of Heavy Objects Suspended With Multiple Cables From a Crane". In: *IEEE Robotics and Automation Letters* 5.4 (2020), pp. 6876–6883. DOI: 10.1109/LRA.2020.3013845.

[12] John Wang and Edwin Olson. "AprilTag 2: Efficient and robust fiducial detection". In: *Proceedings of the IEEE/RSJ International Conference on Intelligent Robots and Systems (IROS)*. Oct. 2016.

[13] Nima Fazeli et al. "Parameter and contact force estimation of planar rigid-bodies undergoing frictional contact". In: *The International Journal of Robotics Research* 36.13-14 (2017), pp. 1437–1454. DOI: 10.1177/0278364917698749. eprint: https://doi.org/10.1177/0278364917698749. URL: https://doi.org/10.1177/0278364917698749.